Nonphotochemical Hole-Burning Study of Selectively Stained Normal and Cancerous Human Ovarian Tissues

S. Matsuzaki,[†,||] J. M. Hayes,[†] D. M. Benbrook,[‡] and R. Jankowiak*[,§]

Department of Chemistry, Iowa State University, Ames, Iowa 50011, Department of Obstetrics and Gynecology, University of Oklahoma Health Sciences Center, Oklahoma City, Oklahoma 73190, and Department of Chemistry, Kansas State University, Manhattan, Kansas 66502

Received: January 6, 2006; In Final Form: April 24, 2006

Results are presented of nonphotochemical hole-burning (HB) experiments on cancerous ovarian and analogous normal peritoneal in vitro tissues stained with the mitochondrial-selective dye rhodamine 800. A comparison of fluorescence excitation spectra, hole-growth kinetics data, and external electric field (Stark) effects on the shape of spectral holes burned in cancerous and normal tissues stained with rhodamine 800 revealed significant differences only in the dipole moment change ($f\Delta\mu$) measured by a combination of HB and Stark spectroscopies. It is shown that the permanent dipole moment change for the $S_0 \rightarrow S_1$ transition of the rhodamine 800 molecules in cancerous tissue is higher than that of normal tissue by a factor of about 1.4. The finding is similar to the HB results obtained earlier for human ovarian surface epithelial cell lines, i.e., OV167 carcinoma and OSE-(tsT)-14 normal cells stained with the same mitochondria-specific dye (Walsh et al. *Biophys. J.* **2003**, *84*, 1299). We propose that the observed difference in the permanent dipole moment change in cancerous ovarian tissue is related to a modification in mitochondrial membrane potential.

1. Introduction

Nonphotochemical hole-burning (NPHB) of numerous dye molecules in various polymers and glasses has been extensively studied to show that NPHB is sensitive to the microenvironment around the dye.[1−7] Hole-burning imaging (HBI), a technique that exploits the inherent nano-environmental sensitivity of NPHB for detecting quantifiable differences between cancerous and analogous normal cells, has been the subject of recent papers.[8,9] The procedural feasibility of HBI as a cancer diagnostic tool was explored in refs 8 and 9, where it was shown that NPHB of intracellular dye molecules could be used to reveal anomalies in subcellular structures. The above studies used two distinct cultured human ovarian surface epithelial cell lines—OV167 carcinoma and OSE(tsT)-14 temperature-sensitive SV40 transfected normal cells—both stained with the mitochondria-specific dye, Molecular Probes MitoFluor Far Red 680 (MF680), commonly known as rhodamine 800. It was demonstrated that quantifiable differences between cancerous and analogous normal cells could be detected.[9]

In earlier studies,[10,11] an analogy was drawn between HBI and magnetic resonance imaging (MRI). This analogy was based on the fact that HBI is used to measure pure dephasing times (T_2*) instead of proton relaxation times (T_1), while both are related to the total dephasing time T_2.[12,13] For example, the measurement of T_2 revealed cellular/tissue anomalies based on the variations of photon echo decay of animal and human tissue samples stained with various rhodamine dyes.[14] Although earlier hole width measurements for cells stained with aluminum phthalocyanine tetrasulfonate (APT) did not successfully differentiate between a carcinoma cell line and a related nondiseased cell line, the two cell lines could be distinguished on the basis of the Stark (St) effect (dependence of the width of the zero-phonon line (ZPL) on an applied electric field $\mathbf{E}_{St}$).

A similar conclusion was reached in refs 8 and 9, where further advances were made with significant differences measured in the areas of burn kinetics and the Stark effect, further suggesting that NPHB has potential as an imaging technique used to reveal subcellular anomalies. For example, a significant difference in the dipole moment change (Stark effect) and different hole-growth kinetics of the zero-phonon hole (ZPH) were found between the OV167 carcinoma (cancer) cells and the OSE(tsT)-14 cells.[8,9] That is, the width of the ZPH was dependent on an applied electric field ($\mathbf{E}_{St}$) with laser excitation ($\mathbf{E}_L$) either parallel or perpendicular to $\mathbf{E}_{St}$. This dependence yielded the permanent dipole moment change associated with the $S_0 \rightarrow S_1$ optical transition of MF680. It was argued that the MF680 molecules sensitive to the Stark effect were preferentially located on the mitochondrial membrane. The difference between the dipole moment change values for the two cell lines was up to ~0.8 D, and the dipole moment change values for the carcinoma cell line were higher at various burning frequencies by a factor of 1.5. In the same papers, the researchers also claimed that the differences in the dispersive growth kinetics of the ZPH found between these cell lines might reflect differences in the structural heterogeneity of the cell lines. That is, the dispersive (distributed) growth kinetics of the ZPHs were found to be significantly different with the OV167 line exhibiting the higher burn efficiency, reflecting greater structural heterogeneity of that cell line. Whether this is the case in the current tissue study remains to be established (vide infra) as the tissue samples themselves have heterogeneous cell compositions.

* Author to whom correspondence should be addressed. E-mail: ryszard@ksu.edu.
[†] Iowa State University.
[‡] University of Oklahoma Health Sciences Center.
[§] Kansas State University.
[||] Present address: Free Radical Biology and Aging Research Program, Oklahoma Medical Research Foundation, 825 NE 13th St., Oklahoma City, OK 73104.

10.1021/jp060114i CCC: $33.50
Published on Web 07/22/2006

Because of these earlier successes in cell experiments, which used MF680 for distinguishing carcinoma cells from normal cells, mitochondria remained the organelle of choice for the following reasons. First, recent research has shown that the mitochondria of cancerous tissues exhibit numerous differences from the mitochondria of normal tissues.[15] For example, there are differences in the membrane potential ($\Delta\Psi_m$) generated by mitochondria as well as morphological differences in shape and size.[16,17] Furthermore, lipophilic cationic dye molecules in the rhodamine/rosamine family of dyes have been found to bind preferentially to mitochondria,[18−22] which can be attributed to the membrane composition (namely, lipids, with a negative inside membrane potential relative to the cytoplasm). The staining specificity of the rhodamine dyes has been ascertained with several fluorescent and confocal microscopy studies.[18−20,23−25] Among these rhodamine dyes, MF680 has an additional advantage of red/far red excitation and emission bands. This is particularly important for in vitro tissue samples to avoid the range of autofluorescence as well as the absorption/emission ranges of pH indicator in the tissue culture media entrapped in the intercellular matrixes. Moreover, it is desirable for the dye molecule to exhibit both a high fluorescence quantum yield as well as efficient NPHB. Despite the difficulty of predicting the NPHB efficiency for any given molecule in a given host, previous work by this group on ionic dye molecules similar to the rhodamine family of dyes predicted a favorable outcome for this requirement.[26]

Early diagnosis of cancer is crucial to patient survival. Patients with early stage cancer confined to a small area have a much better prognosis after treatment than patients with more advanced cancers that have spread throughout the body.[27] Since early stage cancers are small, they are not visible to the naked eye; molecular imaging techniques are used to enhance the ability to identify small numbers of cancerous cells within a field of normal cells. In addition, these detection techniques may also be able to monitor the response of a patient's tumor to treatment. One characteristic of cancer cells that distinguishes them from normal cells is their increased metabolism.[28] Mitochondria are critical components of eukaryotic cellular metabolism and are increasingly active as cancer progresses.[29] Therefore, molecules specifically taken up by the mitochondria could potentially be used to identify cells with increased mitochondrial activity suggestive of precancerous or cancerous conditions. Mitochondria are the primary site of oxygen metabolism in the cell, and mitochondrial dysfunction is associated with cancer.[30] The inner mitochondrial membrane is the site of electron transport in oxidative metabolism. Agents that depolarize the mitochondria membrane potential ($\Delta\Psi_m$) can induce an intrinsic cellular pathway leading to apoptosis.[31]

Research presented here continues, refines, and expands previous cell research on differentiating in vitro tissues. Specifically, we present spectral HB results for tissues stained with a mitochondria-specific dye, MF680. In this work, fresh, not snap-frozen, tissues were chosen, thus preserving the native intracellular structures, morphological state, and mitochondrion respiration for the organelle-specific dye. The normal tissue samples were classified according to their physical distance from the malignant tissue. Three types of minced tissue samples were incubated with MF680: (1) a cancerous ovarian tissue (an adenocarcinoma of ovarian origin, stage 3C), (2) a "near" normal peritoneal tissue (i.e., proximal to cancerous tissue), and (3) a "far" normal peritoneal tissue (i.e., obtained at a distal location to cancerous tissue). It is demonstrated that no significant differences could be detected in the ZPH widths and mean phonon frequencies of sideband holes; the differences in the hole-growth kinetics of cancerous/normal tissues were also negligibly small. In contrast, the Stark measurements revealed significant differences that could be used to distinguish subcellular anomalies of various in vitro tissue samples. Potentially, this approach could even be useful for investigating the mitochondrial membrane potential of tissues.

2. Experimental Section

Tissue Extraction. A patient already scheduled for surgery consented to a tissue extraction procedure approved by the Institutional Review Boards (IRBs) for Research Involving Human Subjects of the University of Oklahoma and Iowa State University. Prior to surgery, the patient's doctor was given three labeled containers filled with sterile minimal essential media (MEM) supplemented with 10% fetal bovine serum and an antibiotic/antimycotic mixture. During the operation, the surgeon removed two 1 cm specimens of normal tissue, i.e., one from an area adjacent to the cancer and another further away from it. These specimens, referred to below as near normal and far normal, respectively, were placed in two separate containers. Another 1 cm specimen of the cancerous tissue was also removed and placed into the third tube for evaluation by a pathologist. After tissue evaluation the tubes were placed immediately on ice and shipped to Iowa State University.

Sample Preparation. All three types of tissues, minced by surgical blades to an average of ~1 mm^3, were stained in a suspension using MF680 at a concentration of 250 nM for 15 min at 37 °C. To create staining conditions similar to earlier cell experiments, MEM supplemented with 15% fetal bovine serum (FBS), penicillin/streptomycin (100 U/mL and 100 μg/mL, respectively), and L-glutamine (2 mM) was chosen as the staining medium. MF680 was initially dissolved in dimethylsulfoxide (DMSO). At concentrations used for staining (after diluting with phosphate buffered saline (PBS) and subsequently MEM), the DMSO component of the staining medium was negligible (~0.001%). After the 15 min incubation, the staining media was removed, and the minced tissues were washed (at 100*g* for 5 min) three times with PBS. The tissue fragments were then resuspended in a freezing medium, which consisted of MEM with 5% DMSO. Aliquots of these samples were transferred to 5 mm o.d. gelatin capsules. The samples were then placed in a freezing container and slow-cooled overnight to −70 °C. This step was taken to avoid the formation of ice at cryogenic temperatures.[30,31] Cell viability was tested with the aforementioned cell lines and found to be ≥90% after thawing.[11] Capsules were mounted and rapidly plunged into helium for all hole-burning studies. Unless otherwise noted, all chemicals were purchased from Sigma, St. Louis, MO.

Laser and Cryostat System. The fluorescence excitation system used has been previously described. Briefly, a Coherent Innova 90-C argon ion laser (Coherent, Santa Clara, CA) was used to pump a CR 699-29 ring dye laser, using LD688 laser dye (Exciton, Dayton, OH). This laser system provides 100−500 mW (with 5 W pumping) of power over a wavelength range of 660−720 nm. Laser intensity was stabilized with an LS100 laser power stabilizer (Cambridge Research and Instrumentation, Cambridge, MA); the laser beam was subsequently expanded with a telescope. The laser was operated in two modes: broad-range continuous scanning without intracavity etalons and short-range scanning with intracavity etalons. The scanning ranges and resolution for the broad-scanning mode were 1000 and 0.1 cm^{-1}, respectively; short-range mode measurements were <1.5 and <0.0003 cm^{-1} (<10 MHz), respectively. A polarizer was used to control laser polarization.

Hole-Burning and Fluorescence Spectroscopy. A series of neutral density absorption filters were used to vary hole-burning and scanning intensities. Scanning laser beam intensities were chosen so as not to alter the spectra. For kinetics curve detection, burn intensities less than 0.4 μW/cm^2 were used, while a decrease in the fluorescence signal was concurrently recorded. Because the fluorescence signal decreases very rapidly during the first few seconds of burning and much slower later, the typical channel time for the first 30 s was 0.1 s. After 30 s, the channel collection time was increased to 1 s. The fluorescence excitation signal was collected with a GaAs photomultiplier tube (PMT) (C659−71; Hamamatsu Photonics, Japan) and photon counter (SR-400; Stanford Research, Sunnyvale, CA). The excitation signal was filtered from the PMT with a 720 nm long-pass filter (720ALP; Omega Optical, Brattleboro, VT). Laser scanning and data collection were done with a PC controlled by in-house software.

Confocal Microscopy. All confocal and time-lapse imaging was performed at the Roy J. Carver Laboratory for Ultrahigh Resolution Biological Microscopy (Iowa State University, Ames, IA). The microscope utilized for both imaging methods was a Nikon Eclipse TE200 with an inverted 60× oil-immersion lens (NA, 1.40; theoretical resolution at 632.8 nm, 0.276 μm). The confocal instrumentation was manufactured by Prairie Technologies, LLC (Middleton, WI). Confocal imaging was performed with a He−Ne laser (632.8 nm) for excitation, with a PMT-based detection system and a pinhole aperture set to 100 μm. All software to control the hardware was by Prairie Technologies utilizing National Instruments LabView 5.1. Tissue section preparation was performed at the Histopathology Laboratory, Department of Veterinary Pathology, Iowa State University (Ames, IA). Bulk tissue fragments (sized ∼0.5 cm^3) of the same ovarian tissue sample utilized for hole-burning studies were frozen within Tissue-Tek O.C.T compound (Sakura Finetek, Torrance, CA) to 77 K and maintained until slicing. Cryomicrotomically sliced, unfixed tissue sections (15 or 30 μm) were mounted on poly-L-lysine (Sigma, St. Louis, MO) treated slides for staining and imaging. To facilitate multiple staining procedures without removing the sample from the microscope, an in-house culture well (volume, ∼0.5 mL) was created and affixed to the glass slides. After being thawed at 37 °C in a culture media, the slices were stained with MF680 again at a concentration of 250 nM for 15 min at 37 °C. All images were collected within 1 h of preparation.

3. Results and Discussion

Confocal Microscopy Image. A confocal microscope image of the cryomicrotomically sliced cancerous tissue sample stained with 250 nM MF680 is presented in Figure 1. One notable feature of the image is the specific highlights of the dye in structured organelles, which most closely resemble mitochondria when compared to other studies dealing with the staining of in situ mitochondria.[17] The sodium azide test described in ref 8 was conducted to rule out the possibility that the MF680 dye was locating preferentially somewhere other than the mitochondria or even entrapped in the intercellular matrixes with this concentration. Briefly, a small amount of sodium azide was added to the sample in PBS while it was being imaged on the microscope. Within several seconds, the fluorescence intensity of the cells, which comprised the tissue, was observed to diminish (data not presented). Sodium azide is a toxin that targets enzyme complex IV in the mitochondrial electron transport chain, supposedly resulting in deterioration of the mitochondrial membrane potential. Since the MF680 dye is cationic and requires the membrane potential to maintain its position within mitochondrial membranes, this observation is the direct result of the MF680 being released by the mitochondria to levels below detection due to the influence of the sodium azide. Other depolarizers of mitochondrial membranes (i.e., carbonyl cyanide *p*-trifluoromethoxyphenylhydrazone (FCCP) and/or dinitrophenol (DNP)) provided similar decreases of the fluorescence signal. In addition, we have shown that FCCP diminishes the MF680 fluorescence signal in human ovarian surface epithelial cells as observed in flow cytometry experiments during the measurement of the mitochondrial membrane potential (data not shown). Therefore, we suggest that the decrease of the fluorescence signal described above is largely the result of depolarization of the mitochondrial membrane rather than a direct quenching effect.

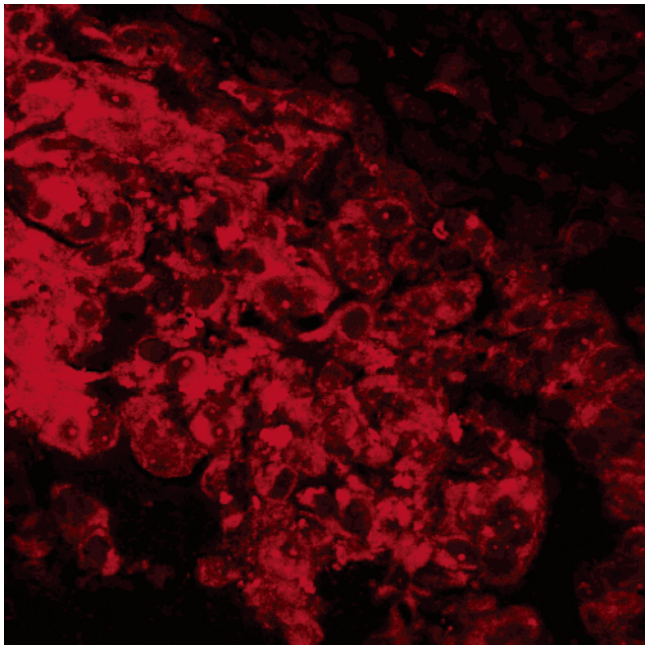

Figure 1. A confocal image of a ∼30-μm-thick cryomicrotomically sliced cancerous tissue sample stained with 250 nM MF680 for 15 min. The white bar represents 20 μm.

Spectra of MF680-Stained Cancerous and Normal Tissues. Fluorescence excitation spectra for MF680-stained cancerous (curve c) and normal tissues (curves a and b) at 5.2 K are given in Figure 2A. The figure also shows the fluorescence excitation spectra of MF680 in hyperquenched glassy water (HGW) (curve d). By comparison of the spectra of MF680 in HGW with that in tissues, a large shift in the fluorescence excitation maxima of the spectra is apparent, signaling dependence on the host matrix, in agreement with previous cell studies.[9] Although the exact cause of these shifts was not a major focus of this study, it is interesting to comment on its possible origin. The absorption and emission maxima in ethanol were measured at 682 and 702 nm, respectively,[32] while the absorption maximum of MF680 in HGW (Figure 2A, curve d) is near 672 nm. None of these matrixes have any lipid nature whatsoever; in each tissue sample, however, the dye molecule is lipophilic and cationic and, as shown in ref 8, is preferentially located in the lipid-based (negatively charged) mitochondria. Another factor was elucidated in the work presented by Sakanoue et al.,[33] who found that on isolated rat liver mitochondria the MF680 dye molecule displayed spectral changes dependent on $\Delta\Psi_m$. The authors made no attempt to explain the shifts, but it is apparent that this molecule's fluorescence excitation is inherently sensitive to $\Delta\Psi_m$ and/or its host matrix composition. The possibility that

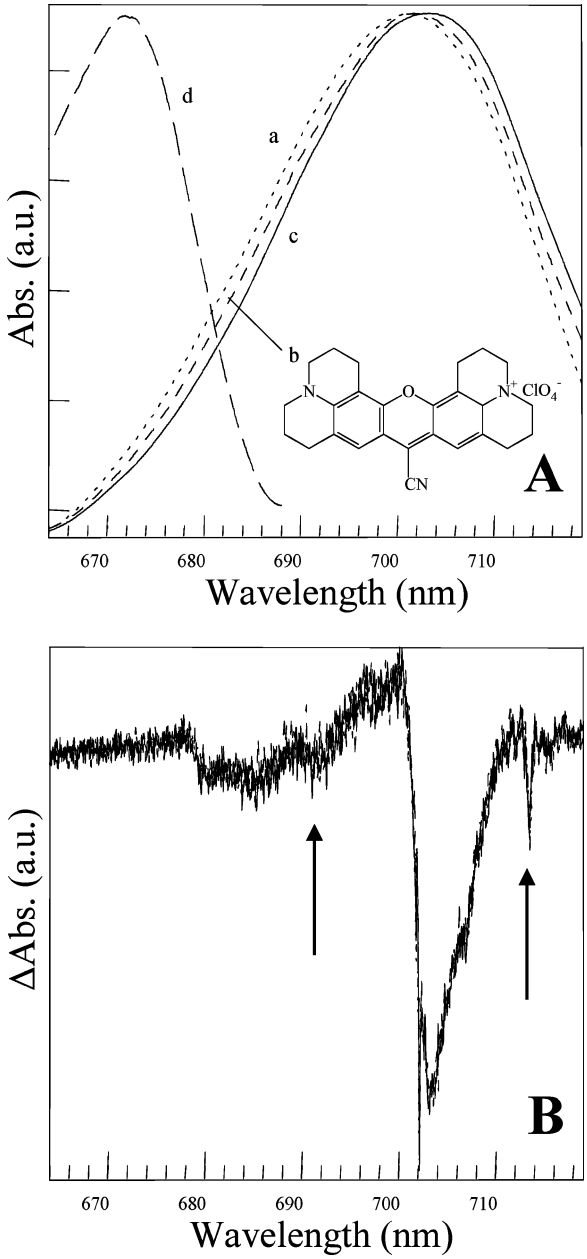

Figure 2. (A) Fluorescence excitation spectra of MF680 in three types of tissue measured at 5.2 K, far normal (dotted line; curve a), near normal (dashed line; curve b), and cancerous (solid line; curve c), in comparison to the fluorescence excitation spectrum of MF680 in HGW (99.9:0.1 (v/v) water/DMSO) (curve d). Note that all the spectra presented were smoothed for purposes of clarification. Peaks are located at ~702, ~701, and ~700 nm, for the cancerous, near normal, and far normal samples, respectively. (B) Representative overlapping (normalized) satellite hole-burned spectra of MF680 in different tissue samples: far normal tissue (dotted line), near normal tissue (dashed line), and cancerous tissue (solid line). The spectra were burned at 702 nm ($T = 5$ K). PSBH is at ~24 cm^{-1} apart from the ZPH, and the most noticeable vibronic peaks on both sides of the ZPH are at 227 cm^{-1} as indicated by the arrows.

the shift is the result of molecular modifications made to the dye in vivo was discounted, as the rat liver mitochondria study revealed reversibility of the MF680 spectral changes dependent on $\Delta\Psi_m$.[33] This indicates that the molecular structure is not being changed. Figure 2B shows three overlapping saturated (normalized) HB spectra burned at 702.0 nm with a fluence of 15 J/cm^2. The depth of the saturated holes shown in Figure 2B is ~32%. The noisy spectra plotted as dotted, dashed, and solid line spectra are indistinguishable. The sharp feature coincident

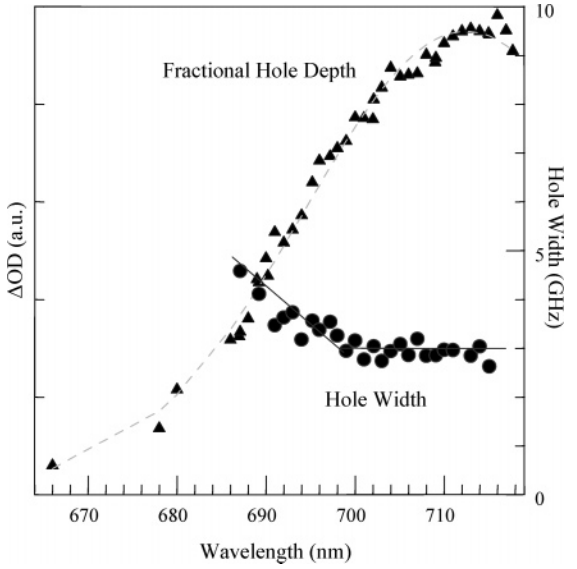

Figure 3. Fractional hole depths and their widths of action spectra of MF680 in cancerous tissue. The dashed line is the Gaussian fit of the fractional hole depth values. Its peak is at ~712.5 nm.

with the burn frequency is the ZPH. On the lower energy side of the ZPH is a pseudo-phonon sideband hole (PSBH). The PSBH is observed to be 24 ± 4 cm^{-1} for each tissue sample with no significant differences in the vibronic satellite hole structures. The latter value is smaller by ~6 cm^{-1} than that observed in cells.[8] The most noticeable vibronic peaks on both sides of ZPH are at 227 cm^{-1} as indicated by the arrows. Moreover, the 372 cm^{-1} mode and the 457 cm^{-1} mode (most likely the overtone of the 227 cm^{-1} vibronic mode) are also observed. The large separation between the ZPH and the PSBH provides favorable conditions to observe hole-growth kinetics for the formation of ZPHs with, in theory, little or no interference from the PSBH.

Hole-Burning Action Spectra. To confirm the predicted distribution of burning species within the absorption band and the homogeneity of the spectral hole profiles, the action spectra of MF680 in the tissue were measured in 1 nm intervals. The fractional hole depths and widths of action spectra, measured with cancerous tissue, are graphed in Figure 3. The light fluence used for the fractional hole depth and hole width measurements of very shallow holes (~5−8%) was far below (by a factor of ~1000) the saturation level. The temperature was 1.8 K. Thus the holes are shallow and not saturated. When hole-burning is initiated at low energies and subsequent holes are then burned at higher energies (i.e., from red to blue), the ability to accurately measure hole depths is greatly diminished[34] due to laser-induced hole filling. Therefore, the reverse process was used: Holes were burned at higher energies with subsequent holes burned at lower energies (i.e., blue to red). As the figure shows, attempts to burn holes in the higher-energy side of the band were unsuccessful because the absorption was increasingly dominated by vibronic/phononic transitions rather than pure electronic transitions, which resembles the action spectra reported earlier for MF680 in cultured cells.[8,9] The Gaussian fit of the fractional hole depths gives a peak of 712.5 ± 0.5 nm, and the hole widths show constant values for burn wavelengths >698 nm. From those facts, wavelengths around 712 nm were chosen for hole-growth kinetics and Stark hole-burning studies, which are discussed later.

Hole-Growth Kinetics. The dispersive kinetics of hole-burning for MF680 in tissues are shown in Figure 4 at two different burn wavelengths (λ_B). These data show only the early

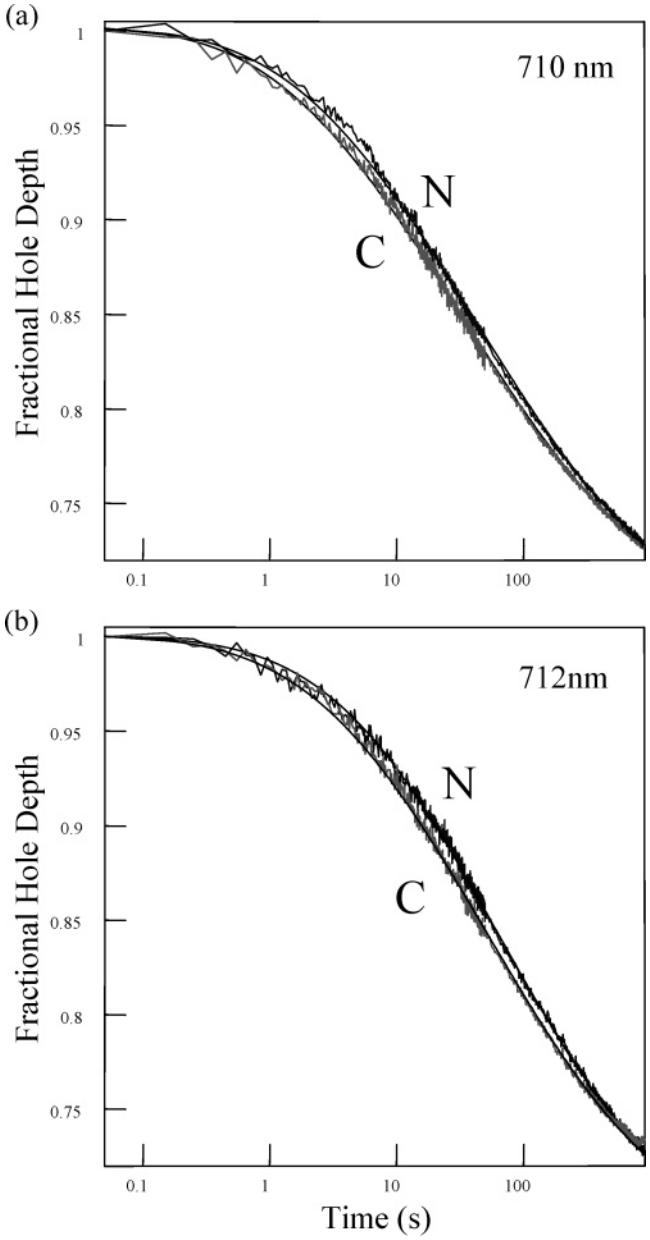

Figure 4. Hole-growth kinetics for MF680 in cancerous (C) and far normal (FN) tissues at (a) λ_B of 710 nm and at (b) λ_B of 712 nm at 1.8 K.

time development of the fractional hole depth and do not refer to the saturated holes. For both, the nonexponential hole-burning verifies that the kinetics cannot be described by a single rate. Using a Gaussian distribution of rates to describe the kinetics has been successful for a variety of glassy samples.[5,35−37] Experimentally obtained kinetic curves were fitted using[38]

$$D(t) = \int d\lambda\, f(\lambda) \int d\alpha \sin\alpha \cos^2\alpha \,(e^{-P\sigma_{LT}{}^{p}\phi(\lambda)\cos^2\alpha t}) \quad (1)$$

where $1 - D(t)$ is the time-dependent fractional hole depth following a burn for time t at a burn ω_B. P is the burn photon flux and was determined from the laser power, taking into consideration the beam size at the sample and attenuating filters in the beam path. α is the angle between the laser polarization and the molecular transition dipole, and $f(\lambda)$ is the Gaussian distribution function of the tunneling parameter λ for the extrinsic two-level systems (TLS_{ext}) active in hole-burning. The unitless parameter λ_0 is the distribution center with a standard deviation σ_λ. Note that the parameters λ and α each define a distribution of hole-burning rates that lead to dispersive kinetics, with the λ distribution being the dominant factor[7,35] accounting for the first 80% of a burn. The parameter $\sigma_{LT}{}^{p}$ is the peak absorption cross-section, for which 2.8×10^{-12} cm^2, a previously determined[8] value for MF680 in cells, was used. The average quantum yield for hole-burning, ϕ, is given by[35,39]

$$\phi(\lambda) = \frac{\Omega_0 \exp(-2\lambda)}{\Omega_0 \exp(-2\lambda) + \tau_{fl}{}^{-1}} \approx \frac{\Omega_0 \exp(-2\lambda)}{\tau_{fl}{}^{-1}} \quad (2)$$

where $\Omega_0 \exp(-2\lambda)$ represents the phonon-assisted tunneling relaxation rate with Ω_0 set to 7.6×10^{12} s^{-1} [40,41] and τ_{fl} is the fluorescence lifetime, again previously determined to be 1.8 ns[8] in an aqueous solution at 77 K. A quantum mechanical expression for Ω_0 can be found in ref 35. The data shown in Figure 4 were fitted to eq 1 by using a three-parameter least-squares fit. The fitting parameters are λ_0, σ_λ, and the fluorescence signal amplitude at $t = 0$ (a technical parameter). For the fits shown (solid smooth lines), the Huang−Rhys factor, S, was set equal to 1.15, based on independent measurements of saturated hole depths, where, in theory, the maximum depth of the saturated ZPH equals $\exp(-S)$. In the fitting procedure, the value of S determines the limiting value of $D(t)$. The obtained values for λ_0 and σ_λ are summarized in Table 1. The values obtained for the far normal (FN) and cancerous (C) tissue samples are quite similar, although the normal tissue samples have slightly higher values for both λ_0 and σ_λ, which is a qualitatively comparable observation to the earlier cell line results.[8]

TABLE 1: Dispersive Hole-Growth Kinetics Fit Parameters for Tissues in Comparison to Those Obtained for Cell Lines[a]

λ_B (nm)	sample	λ_0 (C)	λ_0 (N)	σ_λ (C)	σ_λ (N)
710	tissue[b]	7.05 ± 0.10	7.18 ± 0.10	1.09 ± 0.10	1.14 ± 0.10
	cell[a]	7.78 ± 0.13	8.36 ± 0.12	0.85 ± 0.10	1.10 ± 0.09
712	tissue[b]	7.02 ± 0.10	7.17 ± 0.10	1.09 ± 0.10	1.10 ± 0.10
	cell[a]	7.84 ± 0.10	8.36 ± 0.10	0.68 ± 0.10	1.15 ± 0.08

[a] From ref 8: carcinoma cell line, OV167; analogous normal cell line, OSE14(tsT)-14. [b] Normal (N) tissue samples correspond to "far" normal (FN) peritoneal tissues.

External Electric Field (Stark) Effects. The effects of a 6.0 kV/cm Stark field on the ZPH of MF680 in cancerous and normal tissues at $\lambda_B = 710$ nm are shown in Figure 5 for both parallel (parts a and c) and perpendicular (parts b and d) orientations of the burn laser polarization relative to the Stark field. For all tissue types studied in this work, the Stark broadening was observed for both parallel and perpendicular orientations; however, Stark splitting was not observed in either case. Broadening effects were found to be reversible when the electric field was turned off, thus returning the holes to their original widths while hole depths decreased slightly due to spontaneous hole filling.[36]

A more quantitative comparison of the Stark hole broadening for the three types of tissue samples can be made by calculating the change in dipole moment, $\Delta\mu$. The values of $\Delta\mu$ were determined by fitting a plot of hole width, Γ_h, of the ZPH as a function of applied electric field strength, according to the following equation[42]

$$\Gamma_h(F) = \gamma_0(1 + F^2)^{1/2} \quad (3)$$

where γ_0 is the width of the ZPH at zero field, which includes contributions from both the homogeneous contribution and the

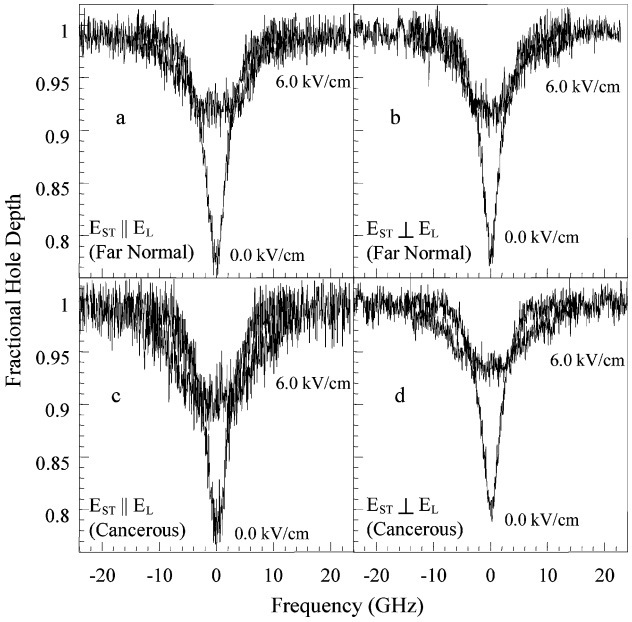

Figure 5. ZPHs, burned at 710 nm, at zero field and with a 6.0 kV/cm external field for MF680 in a far normal tissue sample (parts a and b) and in a cancerous tissue sample (parts c and d) at 1.8 K. Parts a and c correspond to burn laser polarizations parallel to the Stark field, while parts b and d represent laser polarization perpendicular to the Stark field.

TABLE 2: Electric-Field-Induced Permanent Dipole Moment Changes for MF680 in Tissue Samples and Their Ratios[a]

λ_B (nm)[b]	tissue type	$f\Delta\mu$ (D)[c]	$f\Delta\mu$(C)/$f\Delta\mu$(FN)
706	C	2.49 ± 0.06	1.39
	NN	2.18 ± 0.03	
	FN	1.79 ± 0.04	
708	C	2.33 ± 0.06	1.35
	NN	2.01 ± 0.06	
	FN	1.72 ± 0.07	
710	C	2.87 ± 0.03	1.35
	NN	2.42 ± 0.04	
	FN	2.13 ± 0.05	
712	C	2.67 ± 0.04	1.36
	NN	2.51 ± 0.05	
	FN	1.97 ± 0.04	

[a] C = cancerous tissue; NN = near normal tissue; FN = far normal tissue; see text for details. [b] All the data presented in the table are measured with the laser polarization parallel to the Stark field ($\mathbf{E}_{St}$ || $\mathbf{E}_L$). [c] Uncertainties from the fitting procedures.

possible additional contribution from spectral diffusion and/or fluence-induced broadening. F is defined by[42]

$$F = \frac{2f\Delta\mu\mathbf{E}_{St}}{h\gamma} \quad (4)$$

This procedure provides the values of dipole moment changes $f\Delta\mu$, where f is the local field correction, which is unknown for normal and cancerous tissues. Results for these calculations are given in Table 2. An example of the hole width (T = 1.8 K) as a function of applied electric field strength is given in Figure 6 for cancerous (C) and far normal (FN) tissue samples in the parallel orientation ($\mathbf{E}_{St}$ || $\mathbf{E}_L$). A quantitative comparison of the results obtained for the perpendicular polarization was omitted since the values do not exhibit a dependency on the polarization of the applied electric field, as was the case in the results of MF680 in cell lines.[9] From the data in Table 2, it is

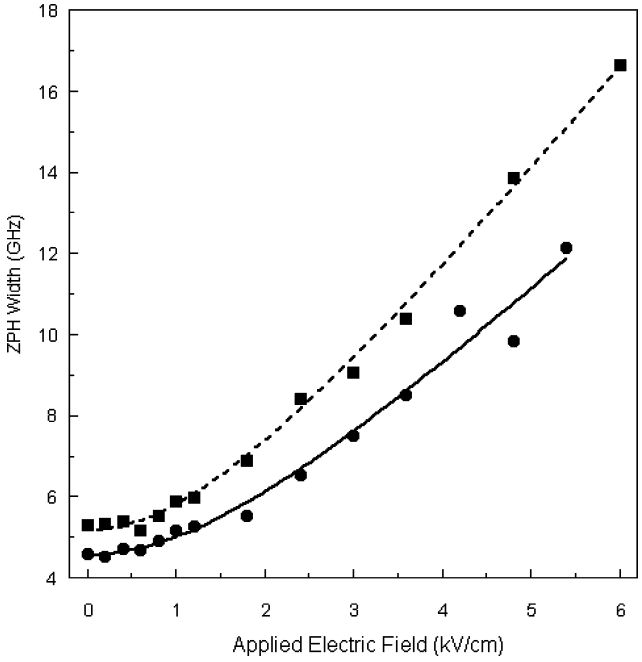

Figure 6. Dependence of hole widths on the strength of the Stark field for MF680 in cancerous (squares) and far normal (circles) tissue samples for a burn laser polarization parallel to the Stark field. Holes were burned at 712 nm. Theoretical fits of Stark broadening are also given for cancerous (dashed line) and far normal (solid line) tissues. T = 1.8 K.

clear that differences in $f\Delta\mu$ values exist between the three tissue samples. Of particular interest is the determination that $f\Delta\mu$ values for the normal tissues are lower than those for the cancerous tissue for all four λ_B values, most likely a result of the lowered $\Delta\Psi_m$ in normal tissues, vide infra. Also of interest is the fact that the ratios of these dipole moment changes $f\Delta\mu$-(C)/$f\Delta\mu$(FN) are ~1.35 for all of the burn wavelengths (with the exception of the λ_B = 706 nm case where a slightly larger value was observed, which still lies well within the bounds of experimental uncertainty).

To understand these results, it must be considered that the change in dipole moment, $\Delta\mu$, is equal to the sum of the intrinsic molecular dipole moment difference, $\Delta\mu_0$, and a matrix-induced component, $\Delta\mu_{ind}$. For the case where $\Delta\mu_0 \gg \Delta\mu_{ind}$, one would expect to observe Stark splitting for one laser orientation and Stark broadening for the other orientation.[43] However, when Stark broadening occurs at both polarizations, where $\Delta\mu_{||} \cong \Delta\mu_{\perp}$, $\Delta\mu_{ind}$ will dominate, thus indicating that $\Delta\mu_{ind}$ is randomly oriented with respect to the transition dipole of MF680 and the laser polarization. Since $\Delta\mu_{ind}$ is composed of a random ($\Delta\mu_r$) and a nonrandom ($\Delta\mu_{nr}$) component, it is expected to vary in a random fashion[45] in agreement with our results. Thus the observation that $\Delta\mu_{||} \cong \Delta\mu_{\perp}$ within each tissue type studied suggests that the overall dipole moment difference is due to matrix-induced factors, and our observations can be explained by specific interaction of the dye molecule with the random environment (most likely mitochondrial inner membrane).

We hasten to add that our results do not exclude any inherent molecular dipole moment change but indicate that this change is smaller than the matrix-induced one and that the splitting (if present) is obscured by broadening. In fact, careful inspection of the holes suggests that some splitting might be there, but it is hidden by broadening to the extent that the Rayleigh criterion is not met. We realize that light propagation in biologic materials thicker than tens of micrometers is typically characterized by multiple scattering events that could lead to partial light

depolarization. However, in our case laser light was only partly depolarized (data not shown), and different laser polarizations burned different fractional hole depths/widths. In addition, the splitting was also not observed in human ovarian surface epithelial cell lines stained with the same specific dye.[8] Thus we conclude that $\Delta\mu_{ind}$ is dominant and only Stark broadening should be observed in agreement with experimental data.

Mitochondrial Membrane Potential. A parameter that we have not elaborated on is the value of $\Delta\Psi_m$. It has been observed in previous studies by other groups[16,18−20,44] that $\Delta\Psi_m$ is greater in magnitude in carcinoma cells/tissues relative to normal cells/tissues. Although the reported values differ depending on the cell lines or origin of the tissue (i.e., 100 mV $\leq \Delta\Psi_m \leq$ 200 mV), the difference in $\Delta\Psi_m$ between carcinoma and normal cell cultures is typically 60−90 mV. Our preliminary data obtained using flow cytometry (unpublished results) indicate that the values of $\Delta\Psi_m$ for the OV167 and OSE(tsT)-14 cell lines are 199.7 and 133.8 mV, respectively. Interestingly, the ratio based on this difference provides a value of ∼1.5 that is similar to the ratio between $f\Delta\mu$ values measured in cell experiments that gave a value of ∼1.5 at λ_B values of 711.8 and 711.6 nm.[9] Although further experimentation is necessary to quantify the differences, it appears that the quantitatively smaller difference of ∼1.4 (Table 2) for tissues instead of ∼1.5 observed for cells is likely related to the inhomogeneity of cell populations that comprise the tissue. However, the discrepancy could also be caused by a different origin of the cells, a different cellular environment, and/or a different stage/kind of carcinoma cells. Nevertheless, we suggest that the difference observed in the permanent dipole moment changes observed in cancerous versus normal tissues is related to a modification in the mitochondrial membrane potential that is an important parameter for mitochondrial functionality and indirect evidence of energy status of the cell.

4. Concluding Remarks.

It has been shown that the permanent dipole moment change for the $S_0 \rightarrow S_1$ transition of the dye in the cancerous tissue was higher than that observed in the normal tissue by a factor of ∼1.35. On the basis of the results of the earlier hole-burning studies of human ovarian surface epithelial cell lines (i.e., OV167 carcinoma cells and OSE(tsT)-14 normal cells[8]), we propose that the difference in the permanent dipole moment change ($f\Delta\mu$) is most likely related to the differences in the mitochondrial membrane potentials of these two tissue types. In contrast to our earlier studies of cancerous versus normal cells,[8,9] the cancerous tissue could not be distinguished from a normal tissue based on the values of the tunneling parameter obtained from the hole-growth kinetics. Nevertheless, the differentiation appears to be possible based on the qualitative as well as quantitative differences found between the cancerous and the normal tissue in the series of experiments utilizing the Stark spectroscopy. We anticipate that, in the future, this approach could allow for differentiating in vitro cancerous versus normal tissues by targeting mitochondria.

Acknowledgment. In memory of Gerald J. Small. This work was supported by the National Science Foundation (Grant No. NSF DMR-9908714) and in part by the National Cancer Institute (Grant No. 2PO1 CA49210-12). The authors thank Robert Doyle for assistance with confocal microscopy experiments.

References and Notes

(1) Walsh, C. A.; Berg, M.; Narasimhan, L. R.; Fayer, M. D. *J. Chem. Phys.* **1987**, *86*, 77.
(2) Kador, L.; Personov, R.; Richter, W.; Sesselmann, T.; Haarer, D. *Polym. J.* **1987**, *19*, 61.
(3) Van den Berg, R.; Völker, S. *Chem. Phys.* **1988**, *128*, 257.
(4) Silbey, R. J.; Koedijk, J. M. A.; Völker, S. *J. Chem. Phys.* **1996**, *105*, 901.
(5) Reinot, T.; Hayes, J. M.; Small, G. J. *J. Chem. Phys.* **1997**, *106*, 457.
(6) Reinot, T.; Hayes, J. M.; Small, G. J. *J. Chem. Phys.* **1999**, *110*, 4820.
(7) Reinot, T.; Small, G. J. *J. Chem. Phys.* **2001**, *114*, 9105.
(8) Walsh, R. J.; Reinot, T.; Hayes, J. M.; Kalli, K. R.; Hartmann, L. C.; Small, G. J. *Biophys. J.* **2003**, *84*, 1299.
(9) Walsh, R. J.; Reinot, T.; Hayes, J. M.; Kalli, K. R.; Hartmann, L. C.; Small, G. J. *J. Lumin.* **2002**, *98*, 115.
(10) Milanovich, N.; Rätsep, M.; Reinot, T.; Hayes, J. M.; Small, G. J. *J. Phys. Chem. B* **1998**, *102*, 4265.
(11) Milanovich, N.; Reinot, T.; Hayes, J. M.; Small, G. J. *Biophys. J.* **1998**, *74*, 2680.
(12) Furusawa, A.; Suga, T.; Kiyoshi, U. *J. Opt. Soc. Am. B.* **1994**, *11*, 1456.
(13) Yaffe, M. P. *Science* **1999**, *283*, 1493.
(14) Djaldetti, M. *Acta Haematol.* **1982**, *68*, 241.
(15) Eapen, C. E.; Madesh, M.; Balasubramanian, K. A.; Pulimood, A.; Mathan, M.; Ramakrishna, B. S. *Scand. J. Gastroenterol.* **1998**, *33*, 975.
(16) Johnson, L. V.; Walsh, M. L.; Chen, L. B. *Proc. Natl. Acad. Sci. U.S.A.* **1980**, *77*, 990.
(17) Chen, L. B.; Summerhayes, I. C.; Johnson, L. V.; Walsh, M. L.; Bernal, S. D.; Lampidis, T. J. *Cold Spring Harbor Symp. Quant. Biol.* **1982**, *46*, 141.
(18) Summerhayes, I. C.; Lampidis, T. J.; Bernal, S. D.; Nadakavukaren, J. J.; Nadakavukaren, K. K.; Shepherd, E. L.; Chen, L. B. *Proc. Natl. Acad. Sci. U.S.A.* **1982**, *79*, 5292.
(19) Davis, S.; Weiss, M. J.; Wong, J. R.; Lampidis, T. J.; Chen, L. B. *J. Biol. Chem.* **1985**, *260*, 13844.
(20) Modica-Napolitano, J. S.; Aprille, J. R. *Adv. Drug Delivery Rev.* **2001**, *49*, 63.
(21) Darzynkiewicz, Z.; Staiano-Coico, L.; Melamed, M. R. *Proc. Natl. Acad. Sci. U.S.A.* **1981**, *78*, 2383.
(22) Leprat, P.; Ratinaud, M. H.; Julien, R. *Mech. Ageing Dev.* **1990**, *52*, 149.
(23) Bassøe, C.-F.; Li, N.; Ragheb, K.; Lawler, G.; Sturgis, J.; Robinson, J. P. *Cytometry, Part B* **2003**, *51*, 21.
(24) Fearey, B. L.; Carter, T. P.; Small, G. J. *J. Phys. Chem.* **1983**, *87*, 3590.
(25) Eltabbakh, G. H. *Minerva Ginecol.*. **2004**, *56* (1), 81.
(26) Stubbs, M.; Robinson, S. P.; Hui, C.; Price, N. M.; Rodrigues, L. M.; Howe, F. A.; Griffiths, J. R. *Adv. Enzyme Regul.* **2002**, *42*, 131.
(27) Chen, Y.; Liu, Z. Y.; Li, R. X.; Guo, Z. *Lymphology* **1999**, *32* (2), 70.
(28) Eng, C.; Kiuru, M.; Fernandez, M. J.; Aaltonen, L. A. *Nat. Rev. Cancer* **2003**, *3*, 193.
(29) Green, D. R.; Reed, J. C. *Science* **1998**, *281*, 1309.
(30) Farrant, J.; Walter, C. A.; Lee, H.; Morris, G. J.; Clarke, K. J. *J. Microsc.* **1977**, *111*, 17.
(31) Franks, F. *J. Microsc.* **1977**, *111*, 3.
(32) Haugland, R. P. *Handbook of Fluorescent Probes and Research Chemicals*, 9th ed.; Molecular Probes: Eugene, OR, 2002; p 487.
(33) Sakanoue, J.; Ichikawa, K.; Nomura, Y.; Tamura, M. *J. Biochem.* **1997**, *121*, 29.
(34) Shu, L.; Small, G. J. *J. Opt. Soc. Am. B* **1992**, *9*, 738.
(35) Kenney, M. J.; Jankowiak, R.; Small, G. J. *Chem. Phys.* **1990**, *146*, 47.
(36) Shu, L.; Small, G. J. *J. Opt. Soc. Am. B* **1992**, *9*, 733.
(37) Kim, W.-H.; Reinot, T.; Hayes, J. M.; Small, G. J. *J. Phys. Chem.* **1995**, *99*, 7300.
(38) Reinot, T.; Small, G. J. *J. Chem. Phys.* **2000**, *113*, 10207.
(39) Reinot, T.; Kim, W.-H.; Hayes, J. M.; Small, G. J. *J. Opt. Soc. Am. B* **1997**, *14*, 602.
(40) Kim, W.-H.; Reinot, T.; Hayes, J. M.; Small, G. J. *J. Chem. Phys.* **1996**, *104*, 6415.
(41) Jankowiak, R.; Hayes, J. M.; Small, G. J. Spectral Hole Burning Spectroscopy in Amorphous Molecular Solids and Proteins. *Chem. Rev.* **1993**, *93*, 1471−1502.
(42) Kador, L.; Haarer, D.; Personov, R. *J. Chem. Phys.* **1987**, *86*, 5300.
(43) Meixner, A. J.; Renn, A.; Bucher, S. E.; Wild, U. P. *J. Phys. Chem.* **1986**, *90*, 6777.
(44) Dairkee, S. H.; Hackett, A. J. *Breast Cancer Res. Treat.* **1991**, *18*, 57.
(45) Vauthey, E.; Holliday, K.; Changjiang, W.; Renn, A.; Wild, U. P. *Chem. Phys.* **1993**, *171*, 253.